ENGLISH VERSION

Investigación del Colapso de un Muro de Mampostería de Ladrillo no Reforzado Bajo Fuerzas de Viento Moderado

Unreinforced Brick Masonry Wall Collapse Investigation Under Moderate Wind Loads

A. Aviram *, J.W. Badillo **, J.A. Prieto [1]**, J.D. Jaramillo **

* Consultora Independiente en Ingeniería Estructural, PERÚ
** Universidad EAFIT, Medellín, COLOMBIA

Fecha de Recepción: 05/07/2018
Fecha de Aceptación: 24/10/2018
PAG 65-80

Abstract

Several methodologies used for the collapse assessment of an unreinforced brick masonry wall subject to out-of-plane bending due to moderate wind loads in Medellin, Colombia are presented. Models include a rigid cantilever model of masonry elements, deformable cantilever and frame models of intermediate concrete columns and beams with and without masonry contribution to the wind resistance, and a finite element model with all concrete frame elements, masonry units and panel openings modeled explicitly. Wind demands are estimated using spatial interpolation of actual wind velocity measurements near the site. Results are presented in terms of peak deflections at the wall top, as well as peak force and stress demand-to-capacity ratios on concrete frames and masonry elements, respectively. Wind pressure distribution, P-Delta effects, interaction and relative contribution to the out-of-plane bending resistance of concrete framing and masonry elements with either one- or two-way action are shown to be the main parameters affecting results, in addition to model selection. Despite significant differences between models, recommended parameters and assumptions lead in all cases to the correct determination of the wall's imminent collapse under the estimated wind demands.

Keywords: *Unreinforced brick masonry, out-of-plane bending, wind loading, wall collapse, slender wall instability*

Resumen

Este artículo presenta varias metodologías analíticas para investigar el colapso de un muro de mampostería de ladrillo no reforzada sujeta a flexión fuera del plano debido a los vientos moderados presentes en Medellín, Colombia. Los modelos analíticos incluyen un modelo rígido de mampostería en voladizo, modelos en voladizo y pórtico de concreto reforzado considerando o excluyendo la contribución de la mampostería, y un modelo de elementos finitos que incorpora explícitamente los pórticos de concreto, las unidades de mampostería y aperturas en los paneles. Las demandas por viento se estimaron por interpolación espacial de las mediciones reales de la velocidad del viento cercanas al sitio. La comparación de los resultados se realiza en términos de las deflexiones máximas en la parte superior del muro, así como las razones de demanda a la capacidad de fuerzas y esfuerzos en los pórticos de concreto y en la mampostería, respectivamente. Se demuestra que la distribución de presiones de viento, efectos P-Delta, interacción y contribución relativa a la resistencia fuera del plano de los pórticos y elementos de mampostería con flexión en una o dos direcciones son los parámetros principales que afectan a los resultados, además de la selección del modelo analítico. A pesar de las diferencias sustanciales entre los modelos analíticos, los parámetros y suposiciones recomendadas resultaron en la correcta determinación del colapso inminente del muro bajo las fuerzas de viento estimadas.

Palabras clave: *Mampostería de ladrillo no reforzada, flexión fuera del plano, fuerzas de viento, colapso de muro, inestabilidad de un muro esbelto*

1. Introduction

On February 21st, 2017, a 6 m tall, 24 m long, and 14 cm thick unreinforced brick masonry wall (brick URM wall) connecting two warehouse buildings in Medellin, Colombia, collapsed under moderate winds. The URM wall was constructed with intermediate, lightly-reinforced, and widely-spaced concrete frames resulting in large masonry panel dimensions. The wall was location in the Centro Industrial del Sur, the main wholesale area of Medellin, Antioquia Department. Falling debris destroyed adjacent parked vehicles and caused disruption in normal labor activities but no injuries were reported. Figure 1 shows the wall prior to and following the collapse, and Figure 2 shows the collapse sequence obtained from a video recording at the Southwest corner.

[1] Corresponding author:
Universidad EAFIT, Medellín, COLOMBIA.
E-mail: jprieto@eafit.edu.co

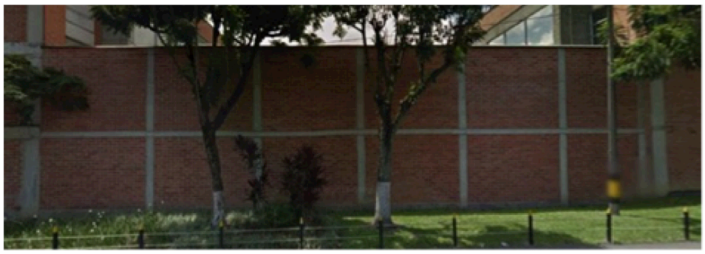

(a) Before the collapse (wall perforations added at later date not shown)

(b) Collapsed wall

Figure 1. *Brick URM wall before and after collapse*

Design calculations were not developed prior to wall construction in 2009, as is customary in the region. Construction drawings and material specifications were not provided by the Contractor for this investigation, and the remaining debris was quickly removed to resume nearby traffic and business operations. Photographic, video, and forensic evidence were available for examination, along with regional wind velocity measurements at the time of collapse. Material strength data was estimated by surveying local brick manufacturers since test data was unavailable due to limited site access and sample set.

Past investigations on the performance of URM walls under dynamic out-of-plane wind demands have been relatively scarce and related work on other masonry structures included support motion simulating earthquake and blast loads (Beak et al. 1994, Griffith et al. 2004, Elsayed et al. 2013). Experimental data on URM walls under out-of-plane demands have therefore primarily been derived from quasi-static and monotonic testing using airbags or multiple load points approximating distributed wind pressures or seismic inertial forces (Drysdale and Essaway 1988, Hoeppner et al. 2002, Doherty et al. 2002, Bean Popehn et al. 2008, Derakshen and Ingham 2008, Vaculik 2012, and Udey 2014). In many of these studies, walls were not cantilevered but rather had two or more supports. Furthermore, tested walls had relatively small dimensions (i.e., length-to-width and height-to-thickness ratios) and were typically treated as rigid or semi-rigid components with idealized pinned supports, whereas the actual site conditions may differ.

Figure 2. *Collapse sequence*

The current study is therefore a unique opportunity to evaluate the adequacy of simplified analytical methodologies to identify the collapse hazard of a long and slender URM wall under dynamic wind loading. Furthermore, video evidence for the collapsed wall shows some degree of rotational restraint at the wall's base and significant curvatures prior to collapse in both horizontal and vertical bending directions, differing from the idealized boundary conditions and assumed deformed shapes used in past studies. Comparison of analysis results is presented in terms of out-of-plane wall deformations and demand-to-capacity ratios (DCRs) in concrete and masonry elements.

2. Wall collapse structural investigation

2.1 Previous Research

The out-of-plane bending resistance of URM walls have been analytically and experimentally investigated by numerous researchers (Drysdale and Essaway 1988, Hoeppner et al. 2002, Doherty et al. 2002, Griffith et al. 2004, Bean Popehn et al. 2008, Derakshen and Ingham 2008, Vaculik 2012, and Udey 2014). In the experimental studies, regardless of the loading method, support conditions, one- or two-way bending response, or wall masonry type, the behavior of all wall specimens shared similar characteristics at failure. The formation of a single, primary crack was obtained in all tests at the masonry-mortar interface, approximately coinciding with the point of maximum bending demand and governing flexural capacity. While the current evaluation utilized global wall displacement estimates, the focus of the above-mentioned studies was localized wall deformations leading to cracking and failure.

Analytical models in the above-mentioned investigations included rigid walls with rocking behavior, semi-rigid walls with arching mechanism, rigid-plastic models, idealized tri-linear force-deformation relations with empirically-derived deformation limits, equivalent linear force-deformation relations matching target displacement limits, and empirically-based flexural resistance formulations, among others. These analytical models were primarily used in static and dynamic response history analyses to predict or calibrate experimental results. Some of these past modeling approaches were also employed in the current study, while others were not applicable due to subjectivity of parameter calibration and lack of material test data.

2.2 Applicable Design Codes

The collapsed URM wall assessment was carried out using local and international design codes. Among them are the Colombian Seismic Resistant Construction Code NSR-10 (MinAmbiente 2010), specifically Title B Loads, Title C Structural Concrete, and Title D Structural Masonry, the Colombian Technical Norm NTC 2289 for reinforcing steel (ICONTEC 2007), and the US codes ACI 318-11 for

reinforced concrete frames (ACI 2011), and TMS 402/602 for masonry design (MSJC 2011).

In this study, the wall system was conservatively categorized as unreinforced masonry instead of confined masonry in-filled in concrete frames due to several reasons: 1) wind loads are imposed in the out-of-plane dimension and concrete frames do not provide confinement under these actions, 2) masonry panel dimensions are relatively large, and 3) there is no beam at the wall top but rather a mortar architectural detail.

2.3 Wall Geometry and Materials

The overall geometry and cross section of the URM wall and intermediate concrete frames presented in Figures 3 and 4 were based on in-situ measurements and observations, and a limited collection of brick samples. The brick unit wall thickness was measured as 1.1 cm on average. Horizontal and vertical mortar joints connecting brick units typically measured between 1-2 cm in thickness.

The resulting height-to-thickness ratio of 40 and length-to-height ratio of 4 were significantly higher than experimentally-tested URM wall specimens found in literature. Per NSR-10, the horizontally-perforated brick units are only allowed for use in unreinforced masonry structures of up to two stories in Occupancy Category I (i.e., low hazard to human life), and were therefore inadequate for use near the adjacent parking area.

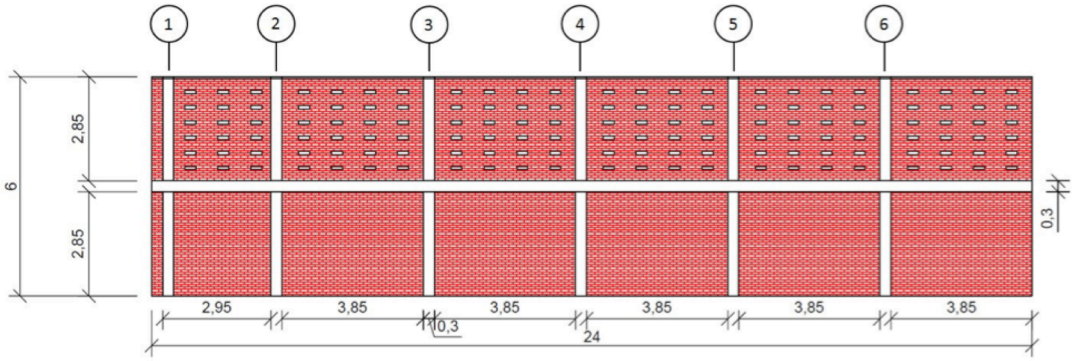

Figure 3. *Wall elevation (measurements in meters)*

Figure 4. *Masonry and concrete frame dimensions and reinforcement.*

The wall perforations shown in Figure 3 were added at an unknown date after the original wall construction (Figure 1), indicating that concern for the poor wind performance of a solid wall had arisen prior to the collapse.

Material strength data for the URM wall was estimated by surveying local brick manufacturers in Medellin. Masonry design strengths widely varied from 3-18 MPa, with low quality units in the range of 3-5 MPa. Due to the lack of formal design calculations and construction details and based on local construction practices for industrial facilities, the masonry design strength, f'_m was estimated at 3 MPa, and the concrete frame design strength, f'_c was estimated at 21 MPA. The corresponding masonry elastic modulus, E_m of 2250 MPa and concrete elastic modulus E_c of 21,530 MPa were calculated per NSR-10. Furthermore, material properties for mortar joints were assumed equal to the masonry units, in lieu of calculating a combined masonry-mortar resistance, since mortar strength data was unavailable and presents a wide range in informal construction. Based on local construction practices, the expected yield strength of longitudinal reinforcement in concrete frames, F_y, was taken as the nominal design strength of 420 MPa per NTC 2289 for ASTM A706 corrugated rebar.

Since column elements and longitudinal reinforcement were shallowly embedded in the ground, fixed boundary conditions were assumed at column bases in some analysis procedures. Conversely, masonry units were not embedded, and pinned supports were used where applicable. Observed shear failure of concrete beams indicated that beam longitudinal reinforcement was not embedded in adjacent buildings, thus pinned supports were applied at beam ends. Significant cracking of concrete frames was evidenced prior to collapse, and even though similar cracking of masonry unit and mortar joints was not explicitly observed from photographic evidence, it is reasonable to assume these also presented considerable degradation due to deformation compatibility with concrete frames.

2.4 Wind Measurements and Spatial Interpolation

Wind measurements for the Medellin region was obtained from SIATA, the local meteorological institute, which records average wind and peak gust velocities and directions every minute of the day in 20 stations. A total of 13 stations presented data from the time of collapse and were used for the wind demand spatial interpolation at the wall site (Table 1). Other nearby stations failed to record wind speeds due to instrument failure and were not utilized. Peak gusts for the applicable stations ranged from 4.5 to 14.2 m/sec during the storm between 3:15 and 5:15 pm and the spatially interpolated peak gust speed at the wall site was determined as 12.3 m/sec. The Open Source Geographic Information Program QGIS Version 2.18.9 was used for wind speed triangular spatial interpolation. Per NSR-10, the Medellin region is located in wind risk category 4 (out of 5) with a basic design wind velocity of 33 m/sec (120 km/h). The estimated peak gust speed at the time of the wall collapse of 12.3 m/sec was clearly well below the design value, indicating the wall was under-designed for wind loads.

Table 1. *Average wind speed and peak gust measurements at time of collapse in nearby stations*

Station ID	Station name	Distance to wall site (km)	Average wind speed (m/sec)	Average gust (m/sec)	Peak gust (m/sec)
59	Isagen	4.6	3.4	5.3	11.7
68	Jardín Botánico	9.9	3.5	6.2	11.5
73	Ciudadela Educativa de la Vida	20.2	4.9	8.4	13.6
82	I.E. Manuel José Caicedo	40.1	3.8	6.2	9.2
83	Centro de Salud San Javier	10.9	2.5	4.5	8.9
84	Escuela Cedepedro	6.5	2.8	4.7	10.4
105	Parque 3 Aguas	11.0	2.5	4.3	11.5
201	Torre SIATA	8.3	6.2	9.3	14.2
202	AMVA	6.7	4.4	7.5	14.2
204	Parque de las Aguas	30.9	4.8	7.7	11.3
205	Santa Elena-Radar	6.8	3.7	4.2	8.9
206	Colegio Concejo de Itagui	6.3	2.5	4.1	9.1
207	Vivero EPM Piedras Blancas	15.3	0.9	1.8	4.5

2.5 Wind Pressure Distributions

Design for wind loads in free-standing walls is carried out in Colombia following NSR-10 Chapter B.6 using either the Simplified or Analytical Procedures. For this study and corresponding site conditions, peak wind pressure was estimated using the Analytical Procedure as $q_{...}$=100 Pa. While in reality a parabolic wind pressure distribution develops on the wall due to increasing wind velocity above ground level,

the pressure distribution used herein was idealized for simplicity as either uniform or triangular. Both distributions, commonly used in past studies, were considered to determine the sensitivity for increased displacement and force demand, while the parabolic distribution was beyond the scope of this work.

2.6 Estimated Wall Deformations

Using video evidence recorded from two different angles at the time of collapse, the wall top peak deflections at incipient collapse were estimated between 15 and 20 cm (Figure 5). Furthermore, the column and masonry wall elements displayed limited rotational restraint at the base, as well as a parabolic deformed shape. The collapse sequence (Figure 2) and debris pattern (Figure 1b) also revealed that once the horizontal supports at the wall ends failed, the masonry wall and concrete frames underwent large displacements and jointly rotated towards the ground.

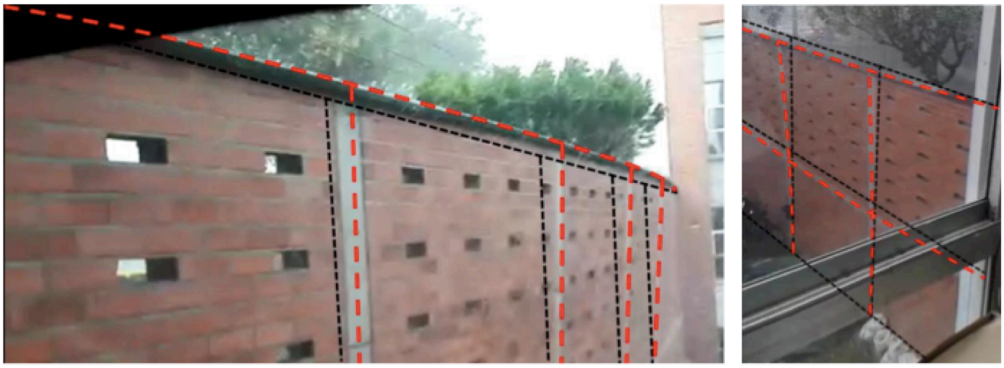

Figure 5. *Wall deformation at incipient collapse seen from two different views (black thin lines indicate original at-rest position. Red discontinuous lines indicate deformed shape at incipient collapse)*

2.7 Analytical Wall Modelling

Several analytical approaches with different basic assumptions and complexity levels were used in the wall collapse investigation to approximate wall out-of-plane deflections and DCRs in concrete frames and masonry elements. The main modeling parameters for each method are presented below and analysis results are tabulated in Section 3 for comparison purposes. A discussion on the benefits and shortcomings of each analysis scheme is also included.

2.7.1 Rigid Cantilever Wall Model

In past investigations, cracked URM walls rocking with large horizontal displacements due to out-of-plane wind or seismic loading have been modeled as rigid blocks separated by fully cracked cross-sections (Doherty 2002, Melis 2002, Willis 2004, Vaculick 2012). This assumption is realistic if there is no vertical pre-compression to deform the blocks, the supports are cracked and allow for simultaneous wall-support rotation, and the dynamic response of the system resembles that of the first mode of vibration. The class of URM walls satisfying such conditions include cantilever walls and simply supported walls spanning vertically, with an additional idealized hinge at mid-height.

In the current study dynamic wind loading is applied as a static force or pressure, using either a triangular or uniform distribution (Figure 6), while inertial forces are ignored. Bending moment equilibrium around the pivot point at the wall base enables the determination of the maximum allowable wind force on the wall before it becomes unstable. At incipient collapse, the wall center of mass is displaced horizontally beyond the projected pivot point, resulting in wall overturning. In this formulation, the displacement capacity is largely a function of wall thickness whereas the strength capacity, assessed separately, is significantly influenced by assumed boundary conditions.

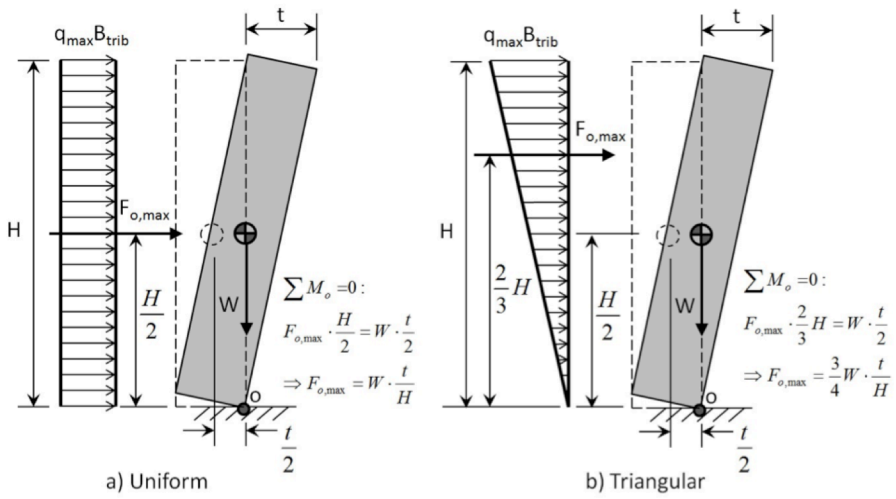

Figure 6. *Rigid Cantilever wall at incipient rocking*

2.7.2 Modelo en voladizo deformable

El modelo en voladizo deformable incluye solamente la resistencia de la columna de concreto, despreciándose la contribución de las unidades de mampostería y la viga a media altura para la rigidez y resistencia del muro. Se asumió que estas columnas estaban completamente fijas en la base y libres para trasferir… y oscilar en la parte superior. Se usaron las propiedades de la sección transversal agrietada para la rigidez a flexión efectiva fuera del plano ya que se observó un agrietamiento significativo antes del colapso del muro. La norma ACI 318-11 recomienda el uso de un factor de reducción de un 0,35 a los elementos de columnas con bajas cargas gravitacionales bajo demandas de flexión; sin embargo, se usó un factor de reducción de 0,25 debido al evidente agrietamiento visible y a la baja razón de refuerzo, es decir:

$$E_c I_{c,effective} = 0.25 E_c I_{c,gross} \quad (1)$$

donde I es el momento de inercia de la columna en la dirección de flexión vertical. Se consideró el ancho tributario en el cálculo de las demandas de viento distribuidas en cada columna como la mitad de la distancia entre las columnas adyacentes. El momento de flexión, de cortante y las demandas de deformación se calcularon usando ecuaciones simples para vigas (Figura 7), mientras que los efectos P-Delta fueron desestimados en este enfoque de modelación simplificado.

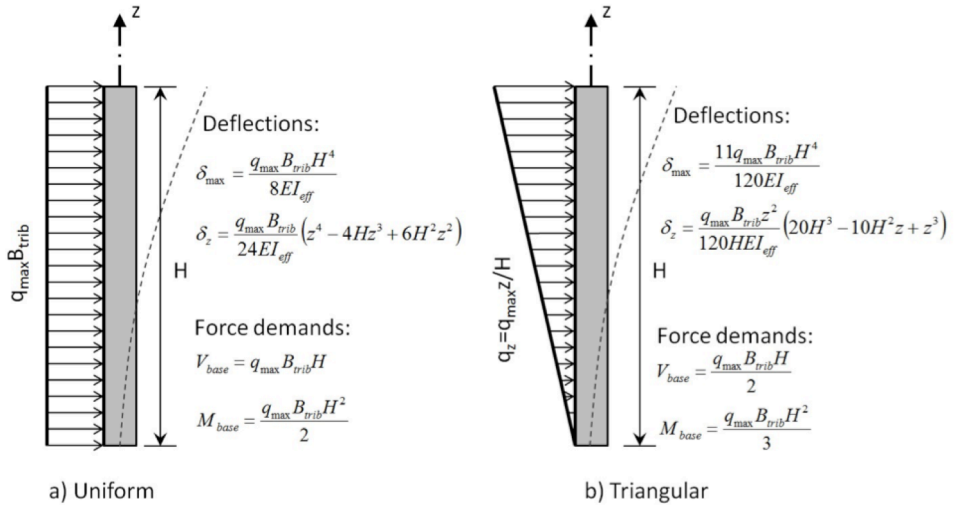

Figure 7. *Force and deformation demands in concrete column in Deformable Cantilever model*

In this model, for a mid-height deflection demand equal to half the wall thickness, the wall top deflection was computed as approximately 20 cm for both uniform and triangular wind loading. This indicates that if column resistance and base fixity were adequate, the wall top could have deflected as much as 20 cm without resulting in overturning due to P-Delta effects.

2.7.3 Frame Models

The horizontal beam contribution to wall out-of-plane bending resistance was examined in the Frame models (Figure 8) using SAP2000 Version 19.2.1 structural analysis program. The Frame Model Without Masonry Contribution (Figure 8a) assumes the concrete frames support the masonry and concrete tributary weight, as well as the tributary wind pressures (Figure 9). The columns were assumed to be fully fixed at the base while the beam was assigned pinned supports at wall ends. Frame element cracked cross section properties were defined similarly as in the Deformable Cantilever model. In the Frame Model with Masonry Contribution (Figure 8b) equivalent masonry frame elements were added in parallel to concrete columns, while masonry contribution to concrete beams was ignored. For the wall bottom half the effective masonry width was taken as 6 times the wall thickness or 85 cm on either side of the column, in accordance with NSR-10 Section D5.4.4 for out-of-plane loading of masonry with running bond. The effective width for the wall top half was estimated as the distance from the column edge and the center of the closest wall openings located or approximately 60 cm on either side of the column. The equivalent thickness of a solid masonry section resisting out-of-plane bending and shear demands was calculated as 10.6 cm from the hollow 14.6 cm deep masonry units in the out-of-plane bending direction and 1 to 2 cm thick vertical mortar joints connecting the units. The masonry elastic out-of-plane bending inertia, I, was significantly reduced in the model by a factor of 0.1, i.e.,

$$E_m I_{m,eff} = 0.1 E_m I_{m,gross} \quad (2)$$

assuming the lack of reinforcement and grouting would lead to significant cracking prior to collapse. Adverse P-Delta effects were included in the analysis, resulting in increased overturning demands due to the wall's self-weight.

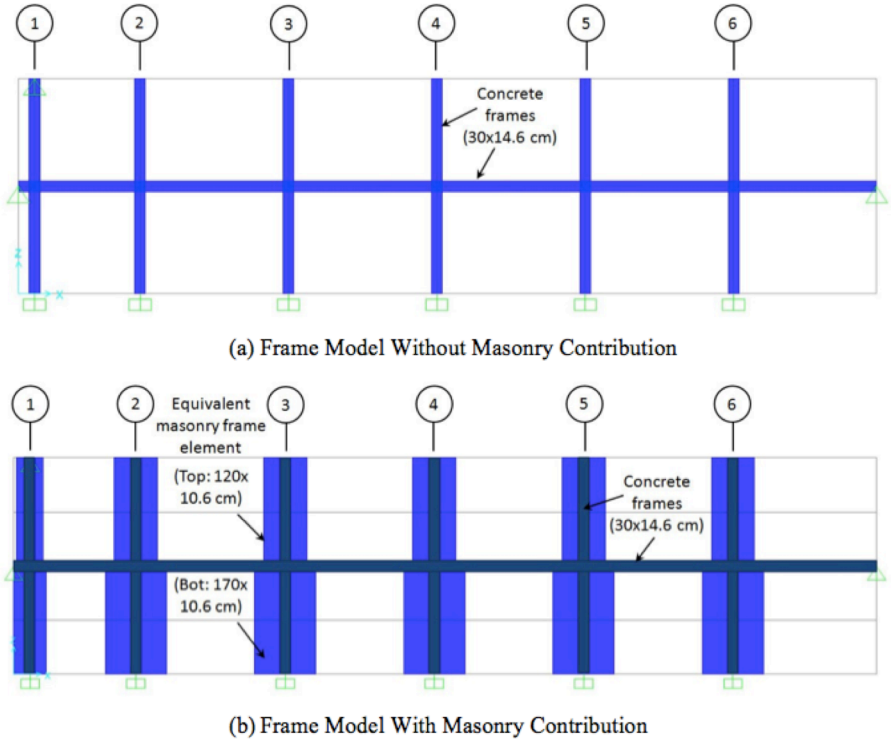

Figure 8. *Rendering of Frame models in SAP2000*

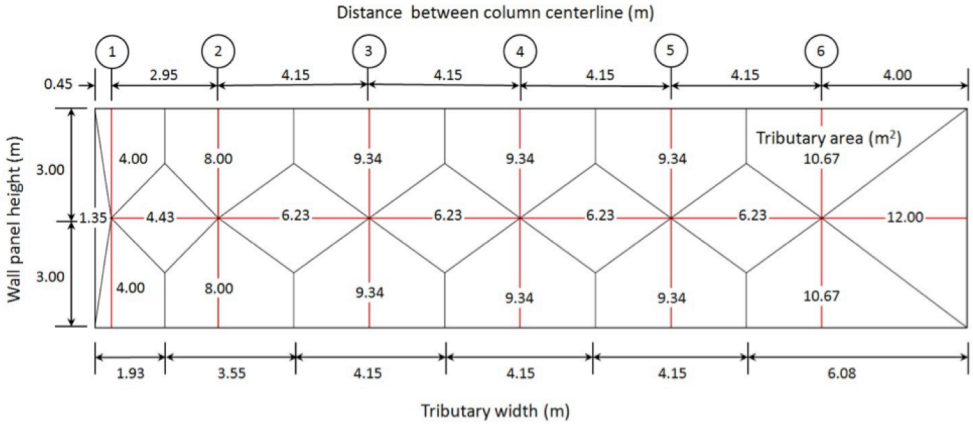

Figure 9. *Tributary widths and areas in the Frame models.*

2.7.4 Finite Element Model

Another method of assessing the contribution of masonry units to wall out-of-plane bending resistance is by modeling them explicitly using finite shell elements connected to concrete frames. The Finite Element Model was investigated using SAP2000 Version 19.2.1 structural analysis program, where the masonry units were assumed to have an effective two-way bending resistance (i.e., m_{11} and m_{22} directions multiplied by 0.1 factor). Membrane response under wind pressures was disregarded (i.e., $f_{11}=f_{12}=f_{22}=0$) since URM walls have negligible resistance in pure tension. Gravity loads corresponding to masonry self-weight (i.e., membrane response in compression) were applied as tributary distributed loads on columns and beams, similar to the methodology used in the Frame models, to include P-Delta effects on the wall overturning demands. The modeling of concrete frames, effective cross section properties, tributary gravity loads, and boundary conditions in the Finite Element model were identical to those used in the Frame models.

The brick masonry finite elements were modeled using shell elements with dimensions similar to the nominal brick dimensions, specifically 30 cm width, 10 cm height, and an equivalent thickness of 11.4 cm. A preliminary mesh sensitivity analysis indicated the selected meshing scheme was adequate. The thickness of the equivalent solid masonry shell elements was determined using a similar methodology to the one employed in the Frame models to match the hollow brick masonry elastic section modulus, including the contribution of mortar joints. However, in the finite element model, the average thickness calculated for the two main bending directions was used (i.e., m_{11} and m_{22}), which presented different cross sections of the hollow brick unit and either horizontal or vertical joints at different spacing.

Wind loading was applied as wind pressure on masonry shell elements using either uniform or triangular distributions, as previously discussed. The masonry was considered pinned at the base and along the entire wall height at both vertical edges for the estimation of peak stress demand at the two end supports, while for the estimation of peak deflections and bending demands of concrete and masonry elements at the wall base, the simple masonry supports at the two vertical ends were removed. Figure 10 shows the Finite Element Model details in SAP2000.

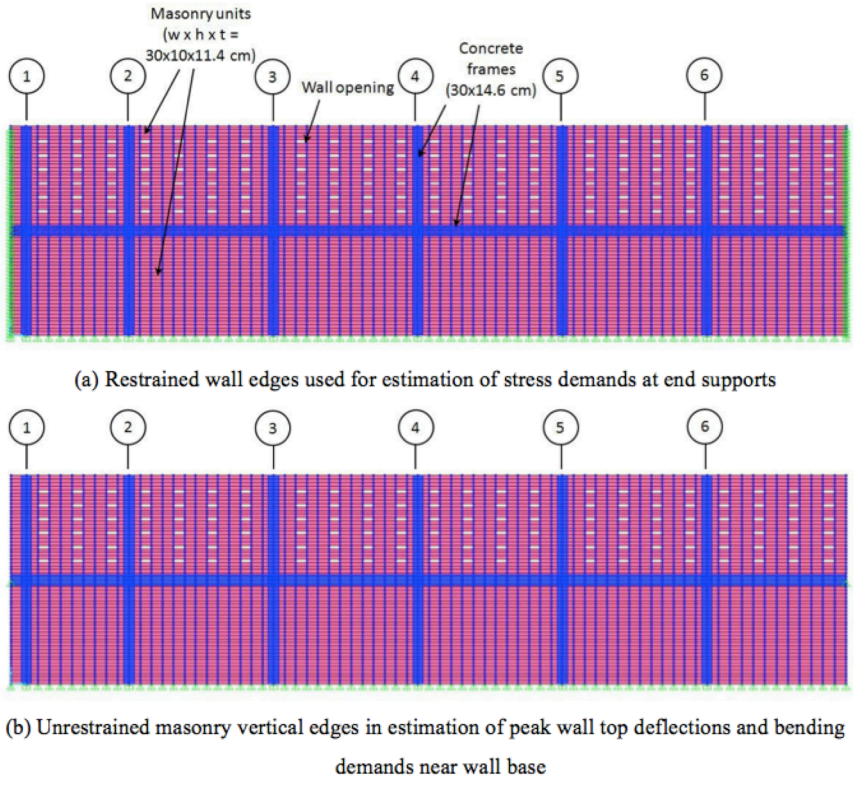

Figure 10. *Rendering of Finite Element models in SAP2000 showing concrete frame and brick masonry element dimensions, boundary conditions, and wall openings in the masonry panels.*

2.8 Wall Capacity

The ultimate concrete column capacity including axial compression, out-of-plane bending moment and shear resistances was calculated using ACI 318-11 and NSR-10 Title C Structural Concrete (Table 2). For axial compression, the assumed lateral restraint conditions and global wall slenderness varied between the different analytical models as previously described. Since P-Delta effects and column slenderness were explicitly included in the Frame model and analysis, the resulting column moment demand magnification was computed directly, while the applied axial load was limited by column cross section axial capacity, as per ACI 318-11. The calculated shear capacity only included the contribution of the concrete section, reduced by half per ACI 318-11, since no transverse reinforcement was provided for out-of-plane bending. The beam's flexure and shear capacities were identical to the column's, and the ultimate axial tensile capacity only included the contribution of steel reinforcement. The frame section capacities approximated for the deformable analytical model (Table 2) conservatively assumed similar boundary conditions for the columns in all models.

Table 2. *Concrete frame capacities*

Analytical Model	***Beam/Column***		***Column***	***Beam***	***Analytical Model***
	Moment (kN-m)	***Shear (kN-m)*** **(kN-m)**	***Slenderness ratio***	**Compresión axial (kN)**	***Moment (kN-m)***
Deformable Cantilever Frame Finite Element	*6.31*	*16.5*	*Kh'/r=300 Sway frame*	*696 (max)*	*106*

The masonry capacity assessment was carried out using NSR-10 Appendix D-1 and the Allowable Stress Design (ASD) method, as specified in NSR-10 for unreinforced masonry (Table 3). The allowable axial stress, F_a, was calculated as

$$F_a = 0.20 f'_m R_e \quad (3)$$

where R_e is the slenderness reduction factor, calculated as

$$\boldsymbol{R_e = 1 - (h'/42t)^2 \quad \text{para } h'/t \leq 30} \quad (4)$$

$$\boldsymbol{R_e = (21t/h')^2 \text{ para } h'/t > 30} \quad (5)$$

In this formulation t is the wall thickness and h' is the effective height between inflection points, taken as 6 m due to the stiffness contribution from the masonry and intermediate beam. The allowable compressive stress due to bending, F_b, was calculated as

$$F_b = 0.33 f'_m \leq 14\ MPa \quad (6)$$

The allowable tensile stress due to bending, F_t, was estimated as 0.10 MPa and 0.21 MPa for stresses perpendicular to horizontal and vertical mortar joints in unreinforced ungrouted masonry, respectively. The allowable shear stress, F_v, was calculated as

$$\boldsymbol{F_v = \left(\sqrt{f'_m}/40 \leq 0.56\ MPa\right) + 0.2 f_{am}} \quad (7)$$

where f_{am} is the compressive stress due to Dead Load.

Table 3. *Unreinforced brick masonry allowable stresses (MPa)*

Analytical Model	F_a	F_b	F_t	F_v
Frame with Masonry Contribution	*0.16*	*0.99*	*0.21 (vertical joints)*	*0.04 (no axial compression)*
Finite Element	(R_e=0.26)		*0.10 (horizontal joints)*	*0.07 (axial compression at base)*

3. Discussion of analysis results

3.1 Peak Deflections

Despite experiencing nonlinear deformations under dynamic wind loading, out-of-plane wall deflections were calculated assuming linear-elastic behavior with an effective stiffness in all models. The wall top peak calculated, and allowable out-of-plane lateral deflections varied between the models (Table 4) due to different modeling assumptions such as deformed shapes and boundary conditions. The tabulated peak deflection results correspond to gridlines 5 and 6 in Figure 3 with the largest tributary widths. The allowable deflection at the wall top corresponded to a mid-height deflection equal to half the wall thickness, beyond which the wall's center of mass contributes to overturning and collapse.

Table 4. *Peak and allowable lateral deflections at wall top*

Model, Pressure Distribution	***Maximum deflection at wall top (cm)***			***Assumed BCs***	***Fails (Y/N)***
	Gridline 5	***Gridline 6***	***Allowable***		
Rigid Cantilever					
Triangular	> * Todos	> * Todos	14.6	*Pinned bottom, free top*	Y
Uniform	** Todos	** Todos	14.6		Y
Deformable Cantilever					
Triangular	13.3	19.6	20,3	*Fixed bottom, free top*	Y
Uniform	18.2	26.7	19,7		Y
Frame Without Masonry Contribution					
Triangular	16.0	16.1	20.3	*Fixed bottom, free top*	N
Uniform	23.6	23.8	19.7		Y
Frame With Masonry Contribution					
Triangular	13.7	13.9	20.3	*Fixed bottom, free top*	N
Uniform	20.3	20.6	19.7		Y
Finite Element					
Triangular	8.4	7.7	11.3	*Pinned bottom, Rotational restraint top*	N
Uniform	11.3	10.6	10.9		Y

* *Allowable deflection resulting in instability reached at* $q=48\ Pa \ll q_{máx}$

** *Allowable deflection resulting in instability reached at* $q=32\ Pa < q_{máx}$

As seen from Table 4, the stiffness contribution of the concrete beam at mid-height in the Frame Model Without Masonry Contribution resulted in an averaged deflection value compared to the results of the Deformable Cantilever model on gridlines 5 and 6 with different tributary widths. The added stiffness of the equivalent masonry frames in the Frame Model With Masonry Contribution resulted in a 15% reduction in lateral deflections, while the two-way bending stiffness of masonry elements in the Finite Element model resulted in a further reduction of 35 to 45% compared to the latter model under triangular and uniform pressures, respectively.

The importance of the pressure distribution assumption is also demonstrated in Table 4; under triangular loading, allowable deflections are not exceeded in the deformable models, whereas under uniform loading wall collapse can be considered imminent. In the Rigid Cantilever model, the instability of the wall is produced under significantly lower wind pressure values than the estimated collapsing pressure at the site, under both triangular and uniform pressures, illustrating the high level of conservatism of this procedure. Using this analytical procedure, a conservative estimate of the maximum wall height remaining stable under a maximum pressure, $q_{\_}$ of 100 Pa, was determined at 2.9 and 1.9 m under triangular and uniform pressure distributions, respectively.

3.2 Demand-to-Capacity Ratios (DCRs)

DCRs for concrete elements were estimated using wind demand results (amplified due to P-Delta effects), assumed to be at the Strength Design (SD) level, and the ultimate capacities summarized in Table 2. Conversely, wind demands for masonry elements were converted to Allowable Stress Design (ASD) level by using a reduction factor of $1/(1.6)^{0.5}$ *per ASCE 7-10 or approximately 0.79 for the different actions assessed (i.e., axial, bending, shear). No load amplification or reduction factors were applied to gravity loads since these were already assumed to be at the ASD level. The governing failure mode corresponded to the action with the highest DCR, and wall failure was determined if controlling DCRs exceeded a value of 1.0. The DCR results obtained for the different models for concrete and masonry elements are summarized in Tables 5 and 6, respectively.*

For masonry elements, the axial compressive stress ratio due to gravity loads was based on hand calculations of tributary axial loads at the base of the wall, not analytical

results from SAP2000. This is significant in the FE model where membrane resistance was not included explicitly.

In the Frame and FE models gridline 5 had slightly higher force demands than column line 6 due to greater bending towards the center of the wall, differing from the results in the Deformable Cantilever model where gridline 6 had a larger tributary area and corresponding wind loading.

As seen from Table 5, for concrete elements, the governing failure mode produced in the models was flexural failure of concrete columns at the base. As seen from the deflection results, triangular pressure loading did not strictly result in collapse, whereas uniform pressure loading did for nearly all models. As seen from Table 6, while flexural stresses near the bottom of gridlines 5 and 6 were comparable between the Frame and FE models, the shear demands in the Frame model were significantly smaller than in the FE model. This is the result of modeling the columns and equivalent masonry elements in parallel in the corresponding Frame model, which allows them to share the lateral wind demand according to their relative stiffness, whereas in the FE model lateral wind loads were primarily applied on masonry shell elements that transfer the load to the columns. Even though shear failure did not govern in most cases, this distinctive behavior may be significant for other wall geometries. The governing failure mode in the masonry varied between tensile and compressive stress due to combined flexure and axial loads and DCRs greater than 1.0 predicting wall failure were produced under uniform pressure distribution.

Table 5. *Demand-to-capacity ratios (DCRs) in concrete framing*

Model, Pressure Distribution	Maximum DCR					Fails (Y/N)
	Col. Axial (P)	Beam Axial (T)	Bending (M)	Shear (V)	Governing DCR, Failure Mode	
Deformable Cantilever (Column 6)						
Triangular	0.02	-	1.16 (Col)	0.11 (Col)	1.16 (M, Col)	Y
Uniform	0.02	-	1.73 (Col)	0.22 (Col)	1.73 (M, Col)	Y
Frame Without Masonry Contribution (Column 5 and Beam)						
Triangular	0.02	0.13	1.01 (Col) 0.41 (Bm)	0.08 (Col) 0.11 (Bm)	1.01 (M, Col)	Y
Uniform	0.02	0.29	1.59 (Col) 0.60 (Bm)	0.16 (Col) 0.17 (Bm)	1.59 (M, Col)	Y
Frame With Masonry Contribution (Column 5 and Beam)						
Triangular	0.01	0.13	0.87 (Col) 0.37 (Viga)	0.08 (Col) 0.11 (Viga)	0.87 (M, Col)	N
Uniform	0.01	0.29	1.38 (Col) 0.55 (Bm)	0.15 (Col) 0.17 (Bm)	1.38 (M, Col)	Y
Finite Element (Column 5 and Beam)						
Triangular	0.01	0.66	0.66 (Col) 0.55 (Bm)	0.27 (Col) 0.08 (Bm)	0.66 (M, Col) 0.66 (T,Bm)	N
Uniform	0.01	0.66	0.99 (Col) 0.24 (Bm)	0.43 (Col) 0.05 (Bm)	0.99 (M, Col)	Y

In the FE model, in addition to the vertical bending of the wall, horizontal bending of masonry panels between column lines also resulted in high stress demands, primarily near the two wall ends near its top (Figure 11 and Table 6). The resulting DCRs predicting failure were higher than those obtained near the bottom of column lines. These results coincided with video evidence showing that the collapse sequence initiated with loss of support at the wall ends.

Table 6. *Demand-to-capacity ratios (DCRs) in masonry elements*

Model, Pressure Distribution	Maximum DCR						Fails (Y/N)
	Axial (f_a/F_a)	Bending-Compr. (f_b/F_b)	Total Compr. ($f_a/F_a+f_b/F_b$)	Bending-Tension (f_t/F)	Shear (f_v/F_v)	Governing DCR, Failure	
Frame with Masonry Contribution							
Column Line 5, Bottom							
Triangular	0.78	0.18	0.96	0.85	0.07	0.96 (M-C)	N
Uniform	0.78	0.29	1.07	1.35	0.18	1.35 (M-T)	Y
Column Line 6, Bottom							
Triangular	0.78	0.16	0.94	0.77	0.02	0.94 (M-C)	N
Uniform	0.78	0.26	1.04	1.24	0.05	1.24 (M-T)	Y
Finite Element							
Column Line 5, Bottom, Vertical Bending							
Triangular	0.78	0.17	0.95	0.82	0.87	0.95 (M-C)	N
Uniform	0.78	0.26	1.04	1.23	1.30	1.30 (V)	Y
Column Line 6, Bottom, Vertical Bending							
Triangular	0.78	0.12	0.90	0.54	0.58	0.90 (M-C)	N
Uniform	0.78	0.18	0.96	0.86	0.91	0.96 (M-C)	N
Column Line 1, Top, Horizontal Bending							
Triangular	-	0.14	-	1.40	0.33	1.40 (M-T)	Y
Uniform	-	0.18	-	1.81	0.43	1.81 (M-T)	Y
Right End, Top, Horizontal Bending							
Triangular	-	0.10	-	1.04	0.36	1.04 (M-T)	Y
Uniform	-	0.14	-	1.40	0.47	1.40 (M-T)	Y

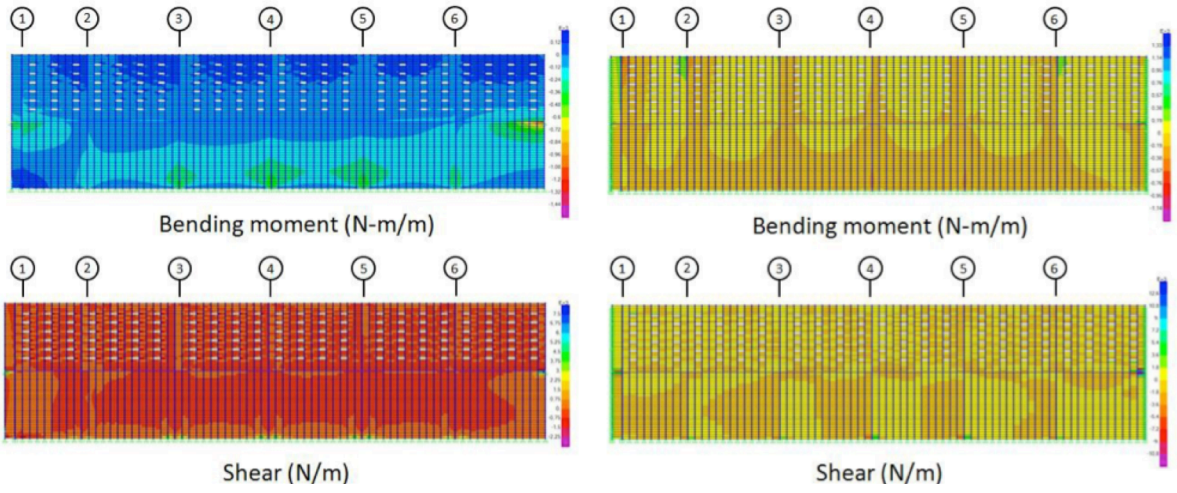

Figure 11. *FE model force results under uniform wind pressure*

4. Conclusion and recommendations

The collapse of a 6 m tall and 24 m long unreinforced brick masonry wall under direct wind loads was assessed using basic analytical approaches and numerous simplifying assumptions to evaluate their efficacy in predicting the observed behavior. Linear static analyses were used to simulate a highly nonlinear dynamic phenomenon by calibration of effective stiffness properties and the idealization of support conditions. These included freely rotating pins for masonry wall edges and foundations, and perfectly fixed supports for concrete column bases. The analyses also included static application of wind pressure distributions and resulted in force and deformations demands that closely approximated available photographic and forensic evidence. Nonetheless, several iterations and parameter variations were required to achieve reasonable precision.

Among the different approaches used, the rigid masonry cantilever wall model with rocking behavior was the most conservative, predicting collapse at wind pressures significantly lower than registered. According to this method, which only required basic wall geometry as input parameters, the maximum wall height of similar construction that would resist collapse was between 2 and 3 meters, a fraction of the actual wall height.

The other analytical models considered were a simple cantilever, frame models of concrete elements with and without masonry contribution to wall out-of-plane stiffness and strength, and a finite element model with two-way bending but no membrane resistance in tension. For these models material properties were conservatively estimated for the brick units, mortar, and concrete framing since test data was unavailable. Effective section properties were used due to considerable cracking observed prior to the collapsing event, specifically $0.25E_c I_g$ for concrete elements, and $0.1E_m I_g$ for masonry under out-of-plane bending. Wind velocities and corresponding wind pressure demands were more accurately estimated through spatial interpolation of actual wind measurements recorded in the region at the time of collapse. Displacement demands at incipient collapse in the order of 15-20 cm and the collapse sequence were determined from several video recordings at the site.

The governing failure modes in the different models consisted primarily of bending failure of concrete columns and exceedance of the allowable compressive and tensile stresses in masonry elements near the wall base. At vertical edges of masonry panels large stresses were also recorded due to horizontal bending between column lines and the wall's high overall length-to-height ratio. DCRs were similar between the different models, with values primarily below 1.0 under a triangular wind pressure distribution and exceeding 1.0 under a uniform distribution. The peak deflection estimation also presented a similar trend, with failure predicted under uniform but not triangular pressure distribution for the different models. Consideration of one- vs. two-way bending of masonry panels in the finite element models proved to be an important modeling parameter since higher stress DCRs resulted from horizontal flexure compared to vertical flexure, which was obviated in the cantilever and frame models.

In general, the wall design proved to be deficient since collapse was predicted by all analysis methodologies considered under moderate wind speeds recorded at the site, which were considerably lower than specified regional design wind speeds. Furthermore, photographic evidence suggests that local engineers or building owners may have already been aware of the design deficiency since wall openings were added after the original construction to relieve wind pressures. Since design calculations were not available for this structure, as is customary in the region, the use of empirical design procedures or regional construction practices should be revised, and conservative design recommendations should be developed for unreinforced masonry walls in industrial facilities and parking structures to prevent future failures.

5. References

ACI (2011), ACI 318-11 Building Code Requirements for Structural Concrete. American Concrete Institute (ACI). Farmington Hills, MI, USA.

ASCE (2010), ASCE/SEI 7-10 Minimum Design Loads for Buildings and Other Structures American Society of Civil Engineers (ASCE). Reston, Virginia, USA.

Beak M., Colwell S.A., Crowhurst D., Ellis B.R. (1994, 19-21 April), The Behaviour of Masonry and Concrete Panels Under Explosion and Static Loading. In Proceedings of I Chem E Symposium Series No. 134, pp. 227-247.

Bean Popehn, J.R., Schultz, A.E., Lu, M., Stolarski, H.K., and Ojard, N.J. 2008, Influence of transverse loading on the stability of slender unreinforced masonry walls. Engineering Structures, 30(10): 2830-2839.

Derakhshan H., Ingham J.M. (2008, 21-23 November), Out-of-Plane testing of an unreinforced masonry wall subjected to one-way bending. In Proceeding of the Australian Earthquake Engineering Conference, Ballarat, Victoria, Australia. Australian Earthquake Engineering Society.

Doherty K., Griffith M. C., Lam N., Wilson J. (2002), Displacement-based seismic analysis for out-of-plane bending of unreinforced masonry walls. Earthquake Engineering and Structural Dynamics, 31(4): 833-850.

Drysdale R.G., Essawy A.S. (1988), Out-of-Plane Bending of Concrete Block Walls. Journal of Structural Engineering, 114(1): 121-133.

Elsayed M., El-Dakhakhni W., Razavi S., Mekky W., Tait M. (2013, 2-5 June), Response of one-way reinforced masonry walls to blast loading. In Proceedings of the 12th Canadian Masonry Symposium, Vancouver, British Columbia, Canada.

Griffith M.C., Lam N.T.K., Wilson J.L, Doherty K. (2004), Experimental Investigation of Unreinforced Brick Masonry Walls in Flexure. Journal of Structural Engineering, 130(3): 423-432.

Hoeppner C.R., Sparling B.F., Wegner L.D., Sakr K. (2002, 5-8 June), CFRP reinforced masonry walls subjected to out-of-plane loading. In Proceedings of 4th Structural Specialty Conference of the Canadian Society for Civil Engineering, Montreal, Quebec, Canada.

ICONTEC (2007), NTC 2289 Barras Corrugadas y Lisas de Acero de Baja Aleación, Para Refuerzo de Concreto- Norma Tecnica Colombiana. Instituto Colombiano de Normas Tecnicas y Certificacion (ICONTEC). Bogota, Colombia.

MSJC (2011), TMS 402-11/ACI 530-11/ASCE 5-11 Building Code Requirements for Masonry Structures and TMS 602-11/ACI 530.1-11/ASCE 6-11 Specification for Masonry Structures. Masonry Standards Joint Committee (MSJC). The Masonry Society, Boulder, CO, USA.

Melis G. (2002), Displacement-Based Seismic Analysis for Out of Plane Bending of Unreinforced Masonry Walls (M.S. Dissertation). Rose School, Pavia.

MinAmbiente (2010), NSR-10 Reglamento Colombiano de Construcción Sismo Resistente. Ministerio de Ambiente, Vivienda y Desarrollo Territorial (MinAmbiente). Asociación Colombiana de Ingeniería Sísmica, Bogotá, Colombia.

SIATA (2017), Sistema de Alerta Temprana de Medellin y el Valle de Aburra (SIATA). https://www.siata.gov.co/sitio_web/index.php/monitoreo#estaciones_meteorologicas.

Udey A. (2014), Realistic Wind Loads on Unreinforced Masonry Walls (M.S. Dissertation). Department of Civil and Geological Engineering. University of Saskatchewan, Saskatoon, Canada.

Vaculik J. (2012), Unreinforced Masonry Walls Subjected to Out-of-Plane Seismic Actions (Ph.D. Dissertation). School of Civil, Environmental & Mining Engineering, University of Adelaide, Australia.

Willis C.R. (2004), Design of Unreinforced Masonry Walls for Out-of-Plane Loading (Ph.D. Dissertation). School of Civil and Environmental Engineering. University of Adelaide, Australia.